

Development of a New Architecture for next Generation e-Bikes

Tiago Gândara¹ ^a and José Santos² ^b

¹*Departamento de Engenharia Mecânica, Campus Universitário de Santiago, 3810-193 Aveiro, Portugal*

²*TEMA-Centro de Tecnologia Mecânica e Automação, Departamento de Engenharia Mecânica, Universidade de Aveiro, Campus Universitário de Santiago, 3810-193 Aveiro, Portugal*

Keywords: e-Bike, System Architecture, Battery Management System, Motor Controller.

Abstract: The growing e-bike market demands more efficient, connected, and user-friendly systems. However, existing e-bike architectures are closed, limiting the integration of new technologies such as power management algorithms and security features. This paper proposes a new system architecture utilizing a microcontroller-based motor controller and CAN bus, allowing integration and data exchange with external devices. Experimental testing was conducted to validate the system's functionality, including testing energy efficiency improvements and security features such as emergency stop protocols. Results demonstrate that the proposed architecture can enhance energy efficiency and provides reliable security, offering a flexible and scalable solution for future e-bike developments.


1 INTRODUCTION


With the increasing popularity of electric bicycles (e-bikes) as a sustainable mode of transportation, the demand for systems tailored to their specific needs has risen. E-bikes offer numerous benefits, including reduced reliance on fossil fuels, decreased urban congestion, and improved accessibility to transportation (Fishman and Cherry, 2016). These advantages have contributed to the rapid growth of the e-bike market. In Europe alone, the market is projected to expand from \$19.36 billion in 2024 to \$29.28 billion by 2029, with a compound annual growth rate (CAGR) of 8.63% (Mordor Intelligence, 2024).

Besides individual ownership, bike-sharing systems have further driven the adoption of e-bikes by offering sustainable and convenient solutions for short-term transportation. Beyond their role in reducing pollution, their minimal space requirements make them an ideal choice for improving quality of life in urban environments (Boglietti et al., 2021). Additionally, studies indicate that 18% to 32% of bike-sharing users would prefer e-bikes if available (Schnieder, 2023).

As e-bikes become integral to urban mobility, their underlying technologies must evolve to address growing user expectations. Recent advancements in e-bike systems have focused on improving user experience, safety, and efficiency. Smart technologies now enable optimized routing to reduce travel times, enhance security with collision sensors, and improve energy efficiency to extend range.

Some authors have focused on developing solutions for bicycle route optimization and data collection. (Nunes et al., 2020) developed an IoT-based module embedded in bicycles to collect real-time sensor data, aiming to enhance cyclists' safety and provide a web-based connectivity platform for route optimization and policy support. (Grama et al., 2018) proposed a modular solution designed to be adapted based on cyclists' needs. The modules focused on two primary functions: measuring bicycle parameters and monitoring environmental conditions. The goal was to develop a platform for collecting and sharing data on air pollution in urban environments. (Andres et al., 2019) used co-operative interaction between the vehicle and the user to get green traffic lights by adjusting the vehicle's speed. (Cammin et al., 2023) introduced a real-time IoT architecture designed to address road traffic challenges by

^a  <https://orcid.org/0009-0004-2040-7155>

^b  <https://orcid.org/0000-0003-0417-8167>

reducing accidents and improving traffic flow through 5G-enabled smart city integration.

Other authors have developed solutions related to increasing the autonomy through optimization of energy consumption. (Arango et al., 2021) developed experimental models for the efficiency of mid-drive motor e-bike components and integrated them into a system-wide efficiency map, maximizing range without compromising speed. (De La Iglesia et al., 2017) developed an intelligent motor management system designed to optimize assistance levels and reduce battery power consumption. The system utilized data from bicycle sensors, historical cyclist data, and neural networks to make informed decisions, resulting in a 10.32% reduction in electricity consumption. (Vishnu et al., 2024) developed a novel control algorithm for a Hybrid Energy Storage System (HESS) that integrates a battery and a supercapacitor and proved that the HESS approach could improve range and performance.

Some authors have also studied collision detection in e-bikes, with advancements in sensor technologies aimed at improving safety and autonomy in complex environments. For instance, (Xie et al., 2021) focused on tracking vehicles at intersections using a narrow, low-density LiDAR system. (Zhao et al., 2017) developed an autonomous bicycle equipped with a high-density three-dimensional LiDAR system, enabling the bicycle to effectively detect and avoid obstacles, showcasing the potential of advanced sensor technologies.

Despite these technological advancements, implementing new systems in e-bikes is challenging due to the prevalence of closed-system architectures. Most e-bikes operate as isolated black boxes, preventing data exchange and integration with external devices. As a result, integrating advanced features often requires additional sensors and microcontrollers, leading to increased system complexity and costs.

As of today, a system architecture that allows for data-sharing, embedded algorithms implementation and easy integration with other modules is yet to be designed. The proposed architecture aims to bridge this gap, providing a flexible foundation for the development and integration of advanced features that enhance performance, safety, and user experience.

1.1 Typical e-Bike Architecture

A typical e-bike architecture consists of several key components including the electric motor, battery,

controller, sensors, human interface, and a battery management system (BMS). The motor, either hub or mid-drive, converts electrical energy into mechanical power, while the battery provides the necessary energy. The controller manages power flow, interpreting input from sensors like pedal-assist and speed sensors to regulate motor output. The human interface, often a display and control buttons, allows riders to adjust power modes and monitor key metrics like speed and battery status. A typical e-bike is shown in Figure 1.

The battery is responsible for powering the whole system. Usually, the battery is composed of lithium-ion cells, which have a nominal voltage of 3.6 volts (V) and are connected in series of 10, 13 or 14, which translate into overall nominal battery voltages of 36V, 46.8V or 50.4V, respectively.



Figure 1: Typical e-bike (Lightmobie, 2025).

To improve the e-bikes range and reduce the electrical current through each lithium cell, typical batteries use parallel connections of cells. By connecting multiple cells in parallel (often in configurations like 3p or 4p), the overall capacity of the battery is increased, allowing for longer ride times and reducing strain on individual cells. The battery management system (BMS) ensures battery safety by preventing overcharging and overheating. The BMS is also responsible for collecting voltage data from all the battery's cells through individual probes. Despite the availability of this data, it is often underutilized, as most motor controllers only acquire limited information, such as overall voltage for state-of-charge (SoC) estimation.

Brushless DC (BLDC) motors are widely used in e-bikes due to their high efficiency, compact size, and

low maintenance. Unlike traditional brushed motors, BLDC motors have no physical brushes, which reduces friction and wear, resulting in a longer lifespan and better performance. The controller is responsible for the motor rotation, which is achieved by switching power to the motor windings in a precise sequence based on rotor position feedback from Hall sensors or sensor-less methods (Xia, C., 2012).

The display is powered by a power line from the controller, usually of 5V. There is also a data line which is used by the controller and the display. This communication is used to exchange information regarding the speed, SoC and level of assistance, and the Universal Asynchronous Receiver Transmitter (UART) protocol is utilized. Figure 2 illustrates a usual e-bike hardware architecture.

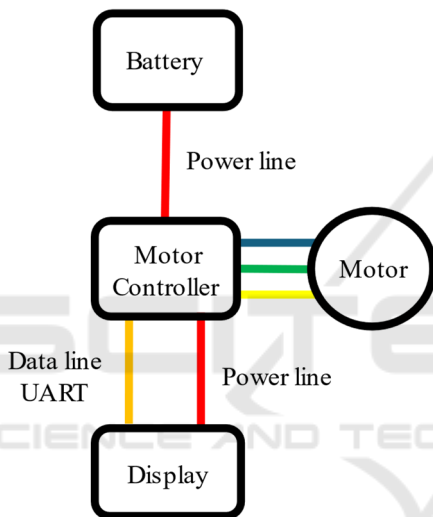


Figure 2: Usual e-bike hardware architecture.

In many current e-bike systems, software-defined assistance levels and speed limits (e.g., 25 km/h per the European Standard EN 15194:2017+A1:2023) dictate performance. However, these systems leave little room for innovation or adaptability to emerging technologies. Therefore, in this paper, a new architecture for any kind of e-bike is proposed.

2 PROPOSED ARCHITECTURE

The proposed architecture is intended to integrate the same type of batteries and motors, differing from the typical architecture only in the controller and display. To facilitate the integration of future devices and technologies, all the information handled by the controller and display must be available to access. Communication systems for e-bikes can be based on

several protocols, each offering different features and capabilities. While some options like FlexRay and automotive Ethernet provide specific benefits for intra-vehicles networks (Tuohy et al., 2015), CAN stands out as the ideal choice for e-bike applications. FlexRay, though fast and fault-tolerant, is too expensive and complex for e-bikes. Automotive Ethernet offers high bandwidth but comes with higher hardware costs. CAN, however, provides a balanced solution with robust performance, real-time communication, scalability, and cost-effectiveness, making it well-suited for integrating subsystems such as motors, batteries, and controllers in e-bikes (Tuohy et al., 2015).

Controller Area Network (CAN) is a robust, message-based communication protocol used for reliable data exchange between multiple devices in real-time, commonly in automotive and industrial systems. It operates on a two-wire bus, where each device (node) can send and receive messages based on priority, ensuring efficient communication. CAN is designed with built-in error detection and fault tolerance, making it highly reliable in noisy environments (Navet and Simonot-Lion, 2008).

As of today, most e-bike battery management systems are only capable of sharing their data through a simple UART communication protocol. Therefore, a secondary device may be needed to receive the data and make it available for other devices in the CAN network (in this case, the controller). For this reason, the proposed architecture utilizes a CAN data bus connecting only the controller and the display, as displayed in Figure 3.

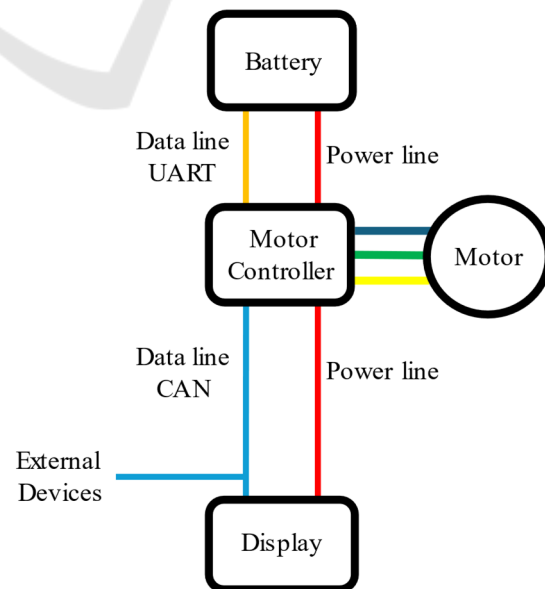


Figure 3: Proposed architecture.

2.1 Controller Architecture

To comply with the requirements of the new architecture, the new controller must be able to establish a UART communication with the BMS, allow for the implementation of energy management algorithms, share and receive data through the CAN network, and offer all the functionalities that regular controllers do. For these reasons, an ESP32 microcontroller was chosen to be the core of the system.

The ESP32 is a low-cost, low-power microcontroller with integrated Wi-Fi and Bluetooth, developed by Espressif Systems. It features a dual-core processor, multiple GPIO pins, and various interfaces (such as SPI, I2C, and UART) that support versatile connectivity and control. It has been shown that ESP32 is an excellent option for embedded systems and smart devices due to the performance properties and price (Maier A. et al., 2017).

2.1.1 Controller Hardware

In this section, the hardware utilized on the controller and its integration is described. As the battery supplies a voltage of at least 36V, and the microcontroller works on either 3.3 or 5V, a voltage regulator is needed to ensure that the proper voltage is supplied to the microcontroller. This voltage regulator is also required to supply any other low-voltage devices on the controller.

As mentioned before, BLDC motor rotation is achieved by switching power to the motor windings in a precise sequence. This switching is usually done with 6 MOSFETs configured in a three-phase bridge arrangement, where each phase of the motor has a pair of MOSFETs (one high-side and one low-side) controlling the current flow. The MOSFETs are switched in synchronization with the rotor position, typically determined by Hall effect sensors, to maintain optimal magnetic alignment and produce continuous rotational force. A microcontroller can detect the motor position in switch power to motor windings correctly, however this method is usually avoided because the microcontroller might not be able to detect the motor's position fast enough when its rotation is high.

An alternative solution is to use a dedicated BLDC motor driver. This device utilizes an analogic integrated circuit to detect the motor's position and switch power accordingly. The motors rotation speed can be controlled by supplying a signal to the driver, typically a Pulse Width Modulation (PWM) signal. Drivers are designed to read the voltage that the PWM

signal generates, and its value must be between 0 and 5 volts. The ESP32's maximum voltage is 3.3V and, therefore, voltage level shifters or optocouplers are required to convert the signals. However, this is not the case if a 5V microcontroller is utilized.

Since the ESP32's CAN controller handles only the digital communication logic, and not the physical transmission, a CAN transceiver is required to convert the logic signals into the differential signals required for the CAN communication. The rest of the e-bike's sensors such as pedal and brake sensors can be connected directly to the microcontroller. Figure 4 is an illustration of all the components that integrate the controller and how they are connected.

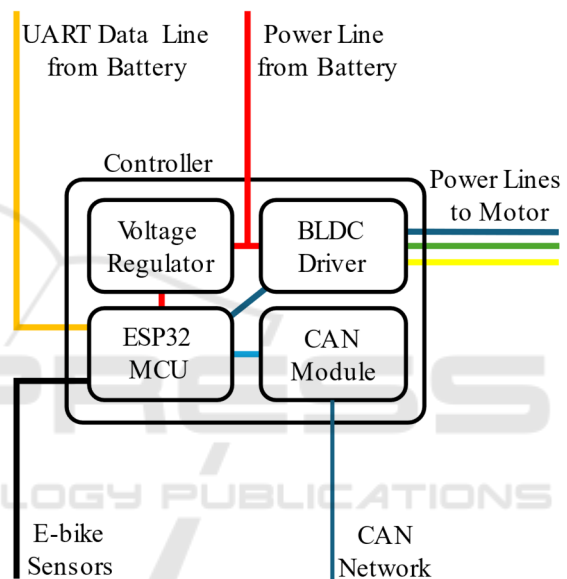


Figure 4: Controller architecture and components.

2.1.2 Controller Software

In order to take full advantage of the ESP32's functionalities, the computational workload was split to run on both CPU cores. Tasks related to speed reading and calculation, pedal and brake sensor reading, and motor driver control run on core 0. Tasks related to communications such as BMS data reading, CAN data reading and CAN data sending run on core 1. This parallelism reduces latency and improves general responsiveness of the system, while simplifying the code structure by assigning specific tasks to each core. Both cores share a common memory, allowing each individual task to access data that was registered by any other task. Figure 5 illustrates the individual tasks, their specific core, and how they're sequenced.

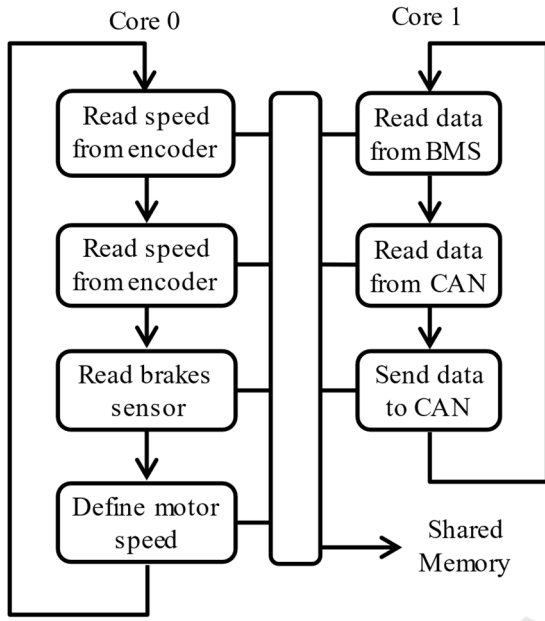


Figure 5: Controller software architecture.

Despite the sequence presented in Figure 5, only some tasks are performed each cycle. For example, if the encoder does not send any pulse to calculate speed, the program will automatically move to the next task. The same concept applies to all tasks.

The encoder sends pulses to the microcontroller every time a specific point of the motor is detected during its rotation. The microcontroller then calculates the time between these pulses to calculate the speed. Every time a pulse is detected, the velocity (v) in meters per second is calculated with the following equation,

$$v = (25.4 \pi D) / [(t_n - t_{n-1}) n_{se}] \quad (1)$$

where n_{se} is the number of encoder position sensors, D is the wheel diameter in inches and $t_n - t_{n-1}$ is the time between pulses in milliseconds. Using just this equation to calculate speed would mean that the speed is not updated in case the vehicle stops. To overcome this, a timeout needs to be set, sacrificing the possibility of reading speeds below a specific speed value. A higher speed value indicates that the controller will be faster to acknowledge the vehicle stopped. Motor with more encoder position sensors will be capable of reading lower speeds than single encoder position sensor motors. Sacrificing the ability to read speeds below 0.56 m/s (2.0 km/h) has proven to be a good balance between speed reading capability and stopping acknowledgement time

during experimental tests. Solving for $t_n - t_{n-1}$ in equation 1, the value of 3703 milliseconds is obtained for a motor with 1 encoder position sensor ($n_s = 1$).

The pedal sensor works in a similar way to the motor encoder. The pedal has a set of magnets that, when in movement, become close to a fixed Hall effect sensor, which sends a signal to the microcontroller. Since the magnets always follow a circular trajectory, the signal becomes a pulse like the encoder output signal. Despite the controller not considering the specific pedaling speed for motor control, the time between pulses is useful to detect when the user starts and stops pedaling. The pedal rotation speed (ω) in rad/s is calculated as

$$\omega = (2000 \pi) / [(t_m - t_{m-1}) n_{sp}] \quad (2)$$

where $t_m - t_{m-1}$ is the time between pulses in milliseconds and n_{sp} is the number of magnets in the pedal sensor. Just like the speed calculation, a timeout value needs to be set to know when the user stopped pedaling. A lower value means the controller will take less to acknowledge the pedals stopped, but the minimum pedal speed will be higher. For a pedal sensor with 12 magnets, experimental tests revealed that a timeout of 750 milliseconds makes a good balance between pedal stopping acknowledgement and minimum pedal speed. Solving for ω in equation 2, an angular speed of 0.70 rad/s.

During discharge, the SoC (in percentage) is calculated through simple segmented functions as

$$SoC = \begin{cases} \frac{8.3V}{n_c} - 23.3, & V < 3.4n_c \\ \frac{150V}{n_c} - 505, & 3.4n_c \leq V \leq 3.7n_c \\ \frac{100V}{n_c} - 320, & V \geq 3.7n_c \end{cases} \quad (3)$$

where V is the measured voltage on the battery terminals and n_c is the number of cells in series. This simplified model was adopted for proof-of concept only, but more complex methods to calculate the SoC can be employed (Hassan et al., 2022).

The braking sensors are installed in both brake levers, and act as normally open switches. Using either the front brake or rear brake will make the controller stop the motor assist immediately. For that reason, the brakes share the same input on the microcontroller, as illustrated on Figure 6.

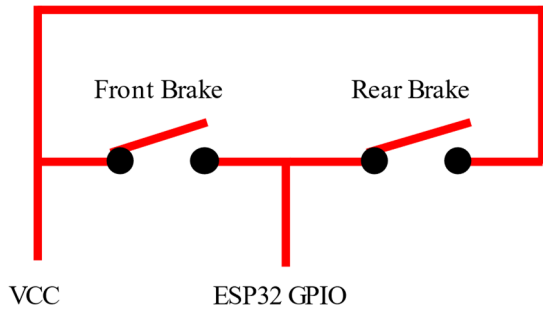


Figure 6: Braking sensors circuit.

The last task that runs on core 0 is the motor speed setting task. Depending on the data collected by the previous tasks, this task will determine the appropriate motor rotation speed. There are 5 different assistance levels, which are chosen by the user with a set of buttons connected to the display. Each assistance level will help the user get to a specific maximum speed, separated by increments of 5 km/h. The motor will only deliver the specific assistance level power if the user is pedaling and not braking. Once the user stops the pedal movement or brakes, the power is interrupted.

There is also the possibility of no assistance at all, usually called 'Level 0'. In this case, the e-bike becomes a regular bicycle, relying only on the user's pedaling to generate motion. In case the user is walking while carrying his e-bike at his side, there is a specific mode called 'Walk mode' (W). This mode will set the motor to a speed of 6 km/h, without the need of pedals to be moving, removing the effort to carry the e-bike around while walking. Table 1 summarizes the different assistance levels and specific max speeds.

Table 1: Assistance levels and velocities.

| Assistance Level | Max Velocity (km/h) |
|------------------|---------------------|
| W | 6 |
| 0 | - |
| 1 | 5 |
| 2 | 10 |
| 3 | 15 |
| 4 | 20 |
| 5 | 25 |

The first task that runs on core 1 is the BMS data retrieving task. The BMS is responsible for monitoring and managing the battery pack to ensure

safe and efficient operation. It balances the charge across individual cells, protects against overcharging, over-discharging, and overheating, and provides data related to all the cells. Depending on the manufacturer and model of BMS, the specific details about the communication protocol may be different, however, the vast majority of BMS provide their data through a standard UART communication protocol.

In this work, the BMS that was utilized for experimental tests only sends data on request. There are two types of requests: When a type 1 request is sent to the BMS, it replies with the overall voltage of the battery, current and temperature. When a type 2 request is sent, the BMS replies with information on the voltages of each cell of the battery. For each type of request, the BMS takes around 100ms to reply with information. Only one request can be processed by the BMS at a time, so the requests are made alternately and the update time for each type of data is 200ms.

The second task running on core 1 is responsible for handling any information arriving from the CAN network and writing it on the microcontroller's internal memory. The only incoming information is the level of assistance that the user selects on the display.

For this work, the CAN protocol J1939 was selected. Developed by the Society of Automotive Engineers (SAE), J1939 standardizes messages, addressing, and diagnostics across vehicle systems, enabling interoperability between components from different manufacturers. It defines message structures, known as Parameter Group Numbers (PGNs), to organize data like engine speed, vehicle speed, and fuel levels, and assigns Suspect Parameter Numbers (SPNs) to specific data points within messages. J1939 is widely used for real-time data sharing, diagnostics, and control in multi-component vehicular systems (Society of Automotive Engineers [SAE], 2023).

Despite not having all the parameters required for e-bikes, the J1939 protocol offers the possibility to use custom PGNs and SPNs. That way, any extra information that is not listed in the protocol can be transmitted through the CAN network. After associating the e-bike's data with the available SPN codes, the custom addresses were created.

The last task running on core 1 is responsible for gathering information from the microcontroller's internal memory and sending it to the CAN network. While some information such as vehicle speed and level of assistance is useful for the display, the rest of the data can be useful for external devices. Table 2 lists the SPN codes and their descriptions.

Table 2: CAN SPN codes.

| SPN | Description |
|-------|---------------------------|
| 84 | Wheel-Based Vehicle Speed |
| 114 | Battery Current |
| 168 | Battery Voltage |
| 521 | Brake Status |
| 3607 | Engine Emergency Shutdown |
| 10001 | Level of assistance |
| 10002 | Controller Temperature |
| 10003 | Battery Temperature |
| 10010 | Cell 1 Voltage |
| 10011 | Cell 2 Voltage |
| 10012 | Cell 3 Voltage |
| 10013 | Cell 4 Voltage |
| 10014 | Cell 5 Voltage |
| 10015 | Cell 6 Voltage |
| 10016 | Cell 7 Voltage |
| 10017 | Cell 8 Voltage |
| 10018 | Cell 9 Voltage |
| 10019 | Cell 10 Voltage |

2.2 Display Module Architecture

Following the same design principle as the controller, the display module architecture adopts an ESP32 as its microcontroller. The display module will be responsible for receiving commands from the user through physical buttons, send and receive data through the CAN network, and display to the user all the important information.

2.2.1 Display Module Hardware

The display module is powered by a power line from the voltage regulator on the controller. Since this work’s objective is only proof of concept, an HMI (Human-Machine Interface) is used to display the relevant information for its ease of use, instead of a regular display. An HMI allows users to interact with the system, using display plus controls like buttons or a touchscreen. A display, in contrast, simply shows information without enabling user input. In this case, the display module will not be taking advantage of the input capabilities of the HMI, as user inputs are received through physical buttons.

A button module with three buttons identical to regular e-bike button module is used. There are two buttons to change the assistance level (Up or Down) and a general-purpose button that allows the user to change settings on the display. In the same way as the controller, a CAN transceiver is necessary to send and

receive messages from the CAN network. Figure 7 illustrates the display module architecture.

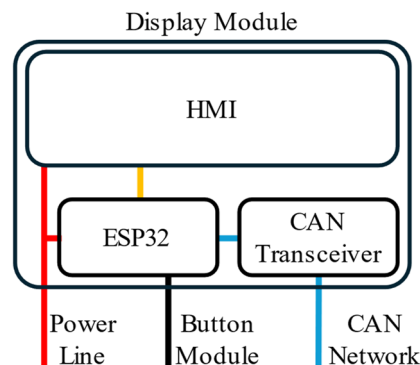


Figure 7: Display module architecture and components.

2.2.2 Display Software

Since the display module computational workload is lighter when compared to the controller’s workload, only core 1 of the microcontroller is used for the display module. Figure 8 illustrates the individual tasks and how they’re sequenced.

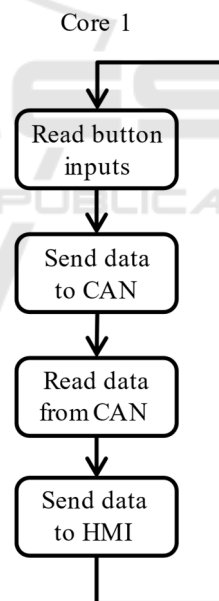


Figure 8: Display module tasks and sequencing.

The cycle begins by reading any inputs from the user through the physical buttons. If the user changes the assistance level, task 2 will take care of sending that information through the CAN network. The third task will check the CAN transceiver module for any incoming data. In case there is new data, then the last task will update the information on the HMI.

The HMI needs to be set up through an application provided by the manufacturers. A set of variables are created and linked to a specific set of pixels on the HMI's display. These variables can then be updated using simple UART communication by the ESP32. Since the HMI's touchscreen is not being used, this communication is not bidirectional, and only the microcontroller sends information to the HMI. The structure of the message sent by the microcontroller may vary depending on the HMI manufacturer. Figure 9 illustrates the set of variables that will be displayed on the screen.



Figure 9: HMI Variables Displayed.

Besides all the information provided by the controller through the CAN network, the HMI displays the instant power draw, total energy draw, distance travelled, and average energy consumption since the trip started. The instantaneous power draw (P) in watts is calculated as

$$P = VI \quad (4)$$

where V is the battery's voltage, and I is the instantaneous current. The total energy (E_t) used in watt-hour (Wh) is calculated with

$$E_t = E_{t-1} + P\Delta t/3600 \quad (5)$$

where E_{t-1} is the previous total energy, P is the current power and Δt is the time between calculations. Every time a new speed is recorded, the distance travelled (x_t) in meters per second is calculated with the previous total travelled distance (x_{t-1}), the vehicle's speed (v) in meters per second and the time between calculations (Δt_v), using equation 5.

$$x_t = x_{t-1} + v\Delta t_v \quad (6)$$

Finally, the average energy consumption (E_a) in watt-hour per kilometer is calculated as

$$E_a = E_t/x_t \quad (7)$$

with the total distance in kilometers, in this case.

3 EXPERIMENTAL TESTS

To test the presented concept, an experimental setup was conceived and built. The conducted experiment's objective is to confirm that the proposed system can replicate the functionality of a regular e-bike, while allowing the implementation of algorithms and communication with external devices that can read the data from the system and send an emergency stop command if necessary.

To conduct the experiment, an e-bike motor was installed in a regular bicycle, and three prototypes were constructed: a controller, a battery with BMS and a display module. An ESP32 with a CAN transceiver was used to simulate an external device. Using 30 individual lithium-ion cells, a battery with BMS was constructed. Figure 10 shows the 3D model in CAD software.



Figure 10: Battery 3D model.

A controller housing was designed to accommodate all the components, and the prototype was 3D printed. The controller assembly was divided into 2 levels. The bottom level of the controller houses the ESP32, the optocouplers module and the BLDC driver. Besides housing the CAN transceiver and the power converter, the top level is also utilized for cable management. In Figure 12 is an illustration of the controller's bottom level in CAD software.

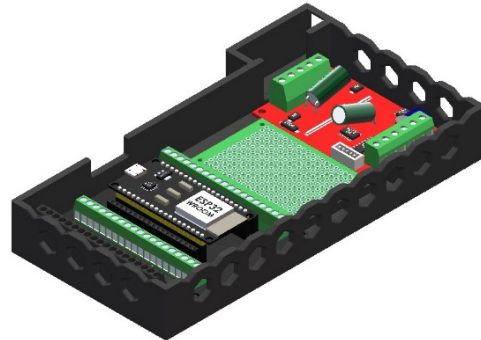


Figure 12: Controller's bottom level.

The display module was assembled and connected to the rest of the system. After assembling all the devices, the experimental setup was complete and experimental testing was possible. Figure 14 shows the whole experimental setup.



Figure 14: Experimental setup.

After building the experimental test setup, several tests were conducted to evaluate the regular functionality of the e-bike and its enhanced features. The first test aimed to verify the basic functionality of the system under normal operating conditions. Initially, assistance level 1 was selected, and the pedals were moved manually. After a few seconds, assistance level 2 was manually selected. Finally, assistance level 3 was selected, and after a brief period, the pedals were brought to a stop, automatically switching the assistance level to 0. The readings were performed by an external microcontroller connected to the bicycle's CAN bus. Measurements of the assistance level and wheel speed were recorded throughout the entire duration of the test, which lasted approximately 11 seconds. The data collected during the first test is presented in Figure 15.

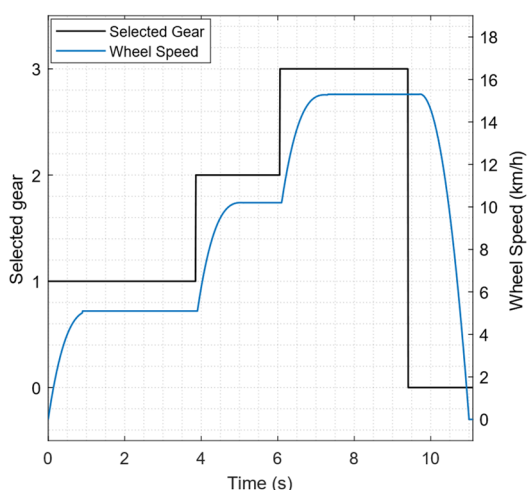


Figure 15: Assistance level and vehicle wheel speed during test 1.

In Figure 15, the plot clearly shows the transition between assistance levels and the corresponding variations in wheel speed, demonstrating the system's ability to adapt to user input in real-time. Since the tests were conducted in a laboratory for proof-of-concept only, the acceleration time between assistance level changes is relatively small. In a real use case scenario, the acceleration time is expected to be substantially larger. When the pedal movement stops, there is a slight delay in the deceleration of the motor. This was expected, since it is related to the acknowledgment time of the pedal's movement stop.

A second test was performed to evaluate the system's response to an emergency stop command issued by an external device, as well as to validate the integrated safety features of the proposed architecture. As a security feature, the controller was programmed to keep the motor disabled even if an emergency stop command is deactivated. This ensures that motor operation cannot resume unintentionally, requiring a full system reset to unlock the motor.

Initially, the assistance level was set to 3, and the pedals were manually rotated to simulate normal operation. An external device then sends a continuous emergency command via the CAN bus which lasts for 2.5 seconds. The values of the emergency stop variable and wheel speed were continuously recorded during the test. The data collected during the second test is presented in Figure 16.

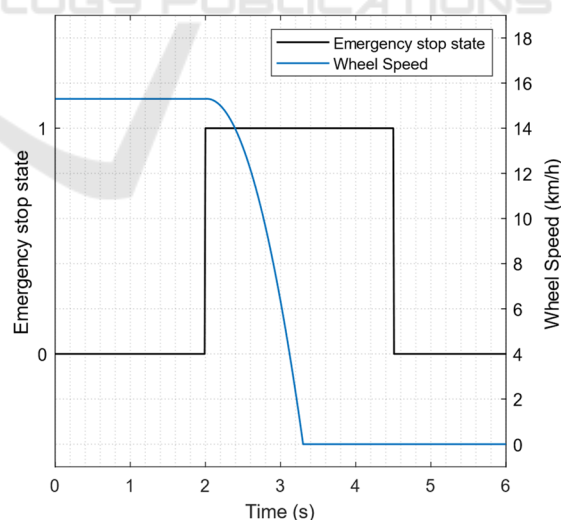


Figure 16: Emergency stop state and vehicle wheel speed during test 2.

The results confirm the system's ability to integrate with external safety mechanisms, since when an emergency command was detected, the

controller immediately halted motor assistance, not resuming motor operation when the emergency state was deactivated.

The final test aimed to demonstrate the potential for improving energy efficiency through the implementation of algorithms. In this test, the electrical current through the motor was first recorded during an acceleration from rest to the speed corresponding to gear 1. The current and wheel speed readings during the acceleration can be seen in Figure 17.

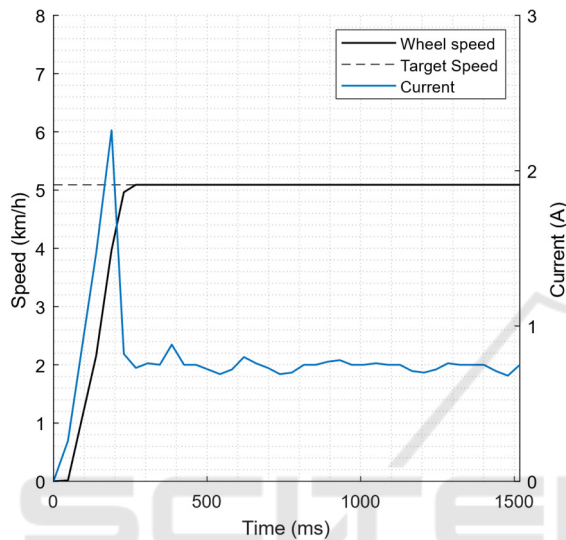


Figure 17: Current and wheel speed reading during regular acceleration.

In this case, when the assistance level is selected and the pedals move, the microcontroller immediately sends a command to the motor driver to achieve the desired speed. The results show an evident current spike which can waste a significant amount of energy.

To eliminate current spikes during accelerations, a simple algorithm is proposed. Instead of sending a fixed speed value to the motor, a simple algorithm can increase the target speed linearly during a specific time interval. For proof-of-concept only, a total time interval of 1 sec was selected for incremental speed increase. For the same final speed (gear 1) as the previous current test, the results of an incremental algorithm can be seen on Figure 18.

As the results from Figure 18 show, utilizing an incremental speed control algorithm has a positive impact on energy consumption, since no current spikes are visible. This example demonstrates the potential to enhance the e-bike's performance through embedded algorithms that can monitor and control not only speed but also other variables like current, temperature and cooling solutions.

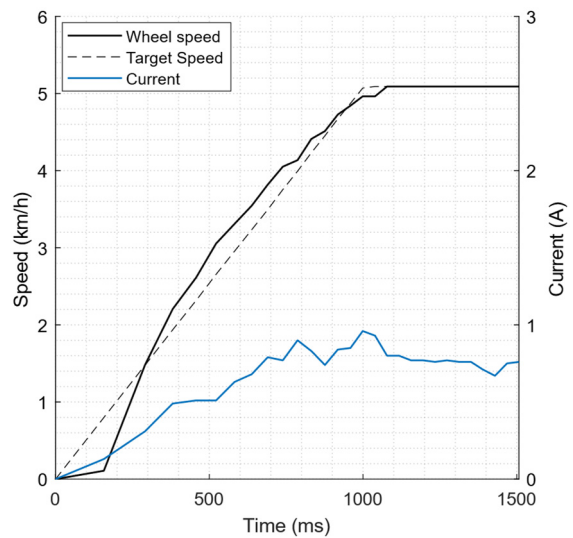


Figure 18: Current and wheel speed reading during incremental acceleration.

4 CONCLUSIONS

In this work, a new architecture for e-bike systems was proposed, centered on an open, microcontroller-based design with a CAN communication bus. This innovative approach addresses the limitations of traditional black-box systems by enabling seamless integration of algorithms, external modules, and subsystems, thereby fostering adaptability and enhanced functionality. Several prototypes were built and used for experimental testing to validate the system's performance and compliance with current e-bike legislation. Testing demonstrated the architecture's practicality, showcasing features such as emergency stop functionality, real-time data sharing, and possibility of implementation of power management algorithms. These results highlight the system's capability to support the evolving demands of urban mobility by offering a flexible, efficient, and connected platform for next-generation e-bike development.

ACKNOWLEDGEMENTS

This work was developed in the scope of the project AM2R – “Agenda Mobilizadora para a Inovação Empresarial do Setor das Duas Rodas” [C644866475-00000012 – Project n. 15], financed by PRR – Recovery and Resilience Plan under the Next Generation EU from the European Union, and by the

projects UIDB/00481/2020 and UIDP/00481/2020 - Fundação para a Ciência e a Tecnologia, <https://doi.org/10.54499/UIDB/00481/2020>.

REFERENCES

- Fishman, E., & Cherry, C. (2015). E-bikes in the Mainstream: Reviewing a Decade of Research. *Transport Reviews*, 36(1), 72–91. <https://doi.org/10.1080/01441647.2015.1069907>.
- Mordor Intelligence (2024), Europe e-bike market - Growth, trends & forecasts up to 2029. Last accessed: January 22, 2025, available at: <https://www.mordorintelligence.com/industry-reports/europe-e-bike-market>.
- Boglietti, S., Barabino, B., & Maternini, G. (2021). Survey on e-Powered Micro Personal Mobility Vehicles: Exploring Current Issues towards Future Developments. *Sustainability*, 13(7), 3692. <https://doi.org/10.3390/su13073692>.
- Schnieder, M. (2023). Ebike Sharing vs. Bike Sharing: Demand Prediction Using Deep Neural Networks and Random Forests. *Sustainability*, 15(18), 13898. <https://doi.org/10.3390/su151813898>.
- Nunes, P., Nicolau, C., Santos, J. P., Completo, A. (2020). From a Traditional Bicycle to a Mobile Sensor in the Cities. In *Proceedings of the 6th International Conference on Vehicle Technology and Intelligent Transport Systems - VEHITS* pages 81-88. <https://doi.org/10.5220/0009349700810088>.
- Gramma, A., Petreus, D., Baciuc, C., Bia, B., Coca, O., Socaciu, V. (2018). Smart Bike Improvement Using Embedded Systems. *2018 41st International Spring Seminar on Electronics Technology (ISSE)*, 1–4. <https://doi.org/10.1109/ISSE.2018.8443769>.
- Andres, J., Kari, T., Kaenel, J.V., Mueller, F.F. (2019). Co-riding With My eBike to Get Green Lights. *Proceedings of the 2019 ACM Designing Interactive Systems Conference*, pp. 1251 – 1263 <https://doi.org/10.1145/3322276.3322307>.
- Cammin C., Mousavi M.R., Trautwein I., Freymann A., Beutelspacher C., Nehrke L., Ludwig S., Kirchheim A. (2023). Concept for a Real-Time IoT-Architecture for Collision Avoidance in Smart Cities based on the 5G Mobile Technology. *2023 IEEE International Conference on Omni-Layer Intelligent Systems*. <https://doi.org/10.1109/COINS57856.2023.10189240>.
- Arango I., Lopez C., Ceren A. (2021). Improving the autonomy of a mid-drive motor electric bicycle based on system efficiency maps and its performance. *World Electric Vehicle Journal*, 12 (2), art. no. 59. <https://doi.org/10.3390/wevj12020059>.
- De La Iglesia, D. H., Villarrubia, G., De Paz, J. F., & Bajo, J. (2017). Multi-Sensor Information Fusion for Optimizing Electric Bicycle Routes Using a Swarm Intelligence Algorithm. *Sensors*, 17(11), 2501. <https://doi.org/10.3390/s17112501>.
- Vishnu S., Dash A., Praveena Krishna P.S., Arjun M., Jayalakshmi N.S. (2022). Hybrid Control Algorithm for BLDC Drive Involving Battery and Supercapacitor in E-bikes. *2022 International Virtual Conference on Power Engineering Computing and Control: Developments in Electric Vehicles and Energy Sector for Sustainable Future*. DOI: 10.1109/PECCON55017.2022.9851060.
- Xie, Z., Jeon, W., Rajamani, R. (2021). Low-density lidar based estimation system for bicycle protection. *IEEE Transactions on Intelligent Vehicles*, 6(1), 67–77. <https://doi.org/10.1109/TIV.2020.3010728>.
- Zhao, M., Stasinopoulos, S., Yu, Y. (2017). Obstacle detection and avoidance for autonomous bicycles. In *2017 13th IEEE Conference on Automation Science and Engineering (CASE)* (pp. 1310–1315). <https://doi.org/10.1109/COASE.2017.8256281>.
- Lightmobie, Lda (2025). Retrieved from: <https://lightmobie.pt/>
- Xia, C. (2012). Permanent Magnet Brushless DC Motor Drives and Controls. Wiley-IEEE Press. ISBN: 9781118188330
- European Committee for Standardization. (2017). EN 15194: 2017 Cycles – Electrically power assisted cycles – EPAC Bicycles. Brussels: CEN.
- S. Tuohy, M. Glavin, C. Hughes, E. Jones, M. Trivedi, L. Kilmartin, (2015) "Intra-Vehicle Networks: A Review," in *IEEE Transactions on Intelligent Transportation Systems*, vol. 16, no. 2, pp. 534-545, , <https://doi.org/10.1109/TITS.2014.2320605>.
- Navet N., and Simonot-Lion F., (2008). Automotive Embedded Systems Handbook. CRC Press. ISBN: 9780849380266
- Maier A., Sharp A., Vagapov Y. (2017). Comparative analysis and practical implementation of the ESP32 microcontroller module for the internet of things. *ITA 2017 - Proceedings of the 7th International Conference*, art. no. 8101926, pp. 143 – 148. DOI: 10.1109/ITECHA.2017.8101926
- Ul Hassan, M., Saha, S., Haque, Md. E., Islam, S., Mahmud, A., Mendis, N. (2022). A comprehensive review of battery state of charge estimation techniques. *Sustainable Energy Technologies and Assessments*, 54, 102801. <https://doi.org/10.1016/j.seta.2022.102801>.
- Society of Automotive Engineers (SEA), (2023). *Serial Control and Communications Heavy-Duty Vehicle Network*. Society of Automotive Engineers.